Journal of Materials Science: Materials in Engineering

RESEARCH Open Access

Green synthesis of zinc oxide nanoparticles using two saffron flower extracts and their comparative photocatalytic efficiency in organic dye degradation

Adil Hamid[1], Mohit Sahni[1*] and Babita Tripathi[1]

Abstract
Zinc oxide (ZnO) nanoparticles are widely explored for photocatalytic degradation of organic pollutants due to their high stability, low cost, and environmental compatibility. In this study, ZnO nanoparticles were synthesized through two green routes using saffron (Crocus sativus) floral extracts to evaluate the effect of extract type and synthesis method on the structural properties and photocatalytic activity. Both saffron anther extract (Z2) and saffron petal extract (Z4) were utilized in the same co-precipitation method to produce green zinc oxide nanoparticles Z2 and Z4. Both approaches avoided toxic reagents, promoting sustainable nanomaterial fabrication. The samples were characterized using X-ray diffraction (XRD), Raman spectroscopy, high-resolution transmission electron microscopy (HR-TEM), and X-ray photoelectron spectroscopy (XPS), confirming the presence of crystalline ZnO with high purity and a nanoscale morphology. Photocatalytic activities were tested under direct natural sunlight using methylene blue (MB), rhodamine B (RhB), and crystal violet (CV) as model dyes. The results revealed that the synthesis route and type of extract significantly influenced degradation performance, with each sample showing dye-dependent activity. The variation in photocatalytic performance between samples synthesized using anther and petal extracts is attributed to differences in phytochemical composition, which influence nucleation behavior and the formation of surface defects. These findings demonstrate the potential of saffron-extract-mediated green synthesis to produce efficient ZnO photocatalysts for environmental remediation.

Keywords Photocatalysis, Green synthesis of nanoparticles, Dye degradation, Wastewater treatment

Introduction

Nanomaterials have garnered considerable attention in recent decades due to their diverse applications across multiple scientific disciplines. The conceptual foundation of nanoscience can be traced back to Richard Feynman's famous 1959 lecture, *"There is Plenty of Room at the Bottom"*, and was later advanced by the invention of the scanning tunneling microscope in 1981, which enabled direct visualization of matter at the nanoscale. According to the International Organization for Standardization (ISO), a nanomaterial is defined as a material with at least one external dimension, internal structure, or surface feature in the size range of 1–100 nm (Benny et al. 2025; Poole-Wilson and Langer 1975). At these dimensions, materials often exhibit unique physicochemical and optoelectronic properties compared to their bulk

*Correspondence:
Mohit Sahni
mohit.sahni@sharda.ac.in

Full list of author information is available at the end of the article

© The Author(s) 2026. **Open Access** This article is licensed under a Creative Commons Attribution 4.0 International License, which permits use, sharing, adaptation, distribution and reproduction in any medium or format, as long as you give appropriate credit to the original author(s) and the source, provide a link to the Creative Commons licence, and indicate if changes were made. The images or other third party material in this article are included in the article's Creative Commons licence, unless indicated otherwise in a credit line to the material. If material is not included in the article's Creative Commons licence and your intended use is not permitted by statutory regulation or exceeds the permitted use, you will need to obtain permission directly from the copyright holder. To view a copy of this licence, visit http://creativecommons.org/licenses/by/4.0/.

Graphical Abstract

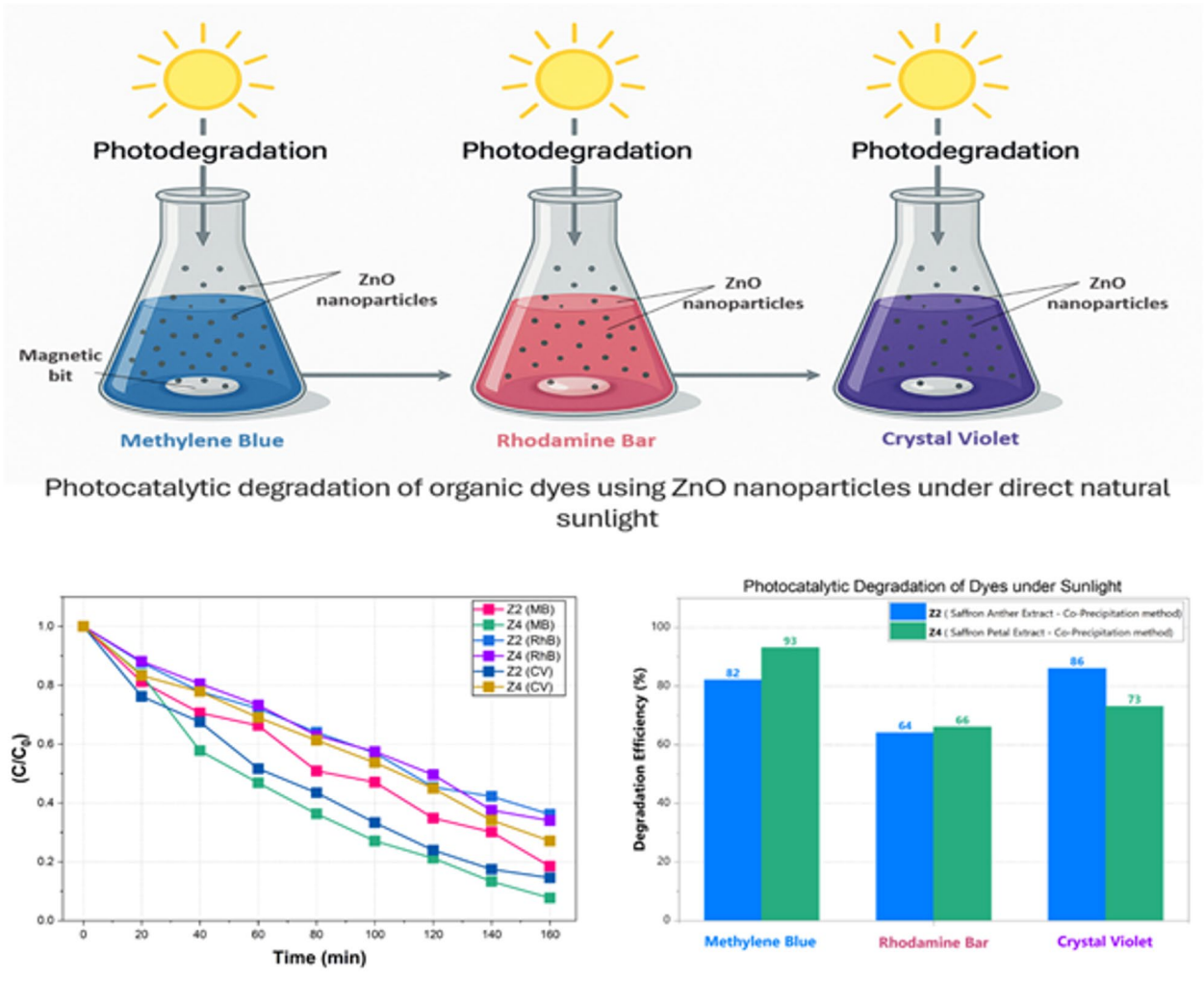

counterparts, which makes them attractive for diverse applications.

Among nanomaterials, transition metal oxides constitute a particularly important class due to their variable stoichiometry, multiple phases, and versatile functional properties. Zinc oxide (ZnO), an II–VI semiconductor, is one of the most extensively studied metal oxides because of its tunable electronic structure, optical transparency, wide bandgap, and rich defect chemistry (Rashad et al. 2016; Weldegebrieal et al. 2023). These properties have enabled ZnO to be applied in areas such as photocatalysis, sensors, medicine, personal care products, paints, batteries, solar cells, memory devices, spintronics, and even agriculture, where it is used to control crop diseases and as a biofertilizer (Ogunyemi et al. 2019; Chaudhuri et al. 2017; Umar and Hahn 2010). A detailed overview of these applications can be found in the reference (Kołodziejczak-Radzimska and Jesionowski 2014a; Varshney et al. 2022).

In addition to these technological uses, ZnO has also gained attention for its role in environmental remediation. Its chemical stability, biocompatibility, and biodegradability make it an effective photocatalyst and antibacterial agent (Baruah et al. 2010; Singh et al. 2025). One of the most pressing global challenges is the treatment of industrial wastewater contaminated with persistent organic pollutants, such as synthetic dyes (Buapoon et al. 2021; Mohammadi Azar et al. 2022). Rapid industrialization, particularly in sectors such as textiles, leather, paper, and ink, has significantly increased the discharge of dye effluents into water bodies, resulting in ecological and human health hazards. Azo dyes, in particular, are widely used in the textile industry, and a substantial fraction—ranging from 10–15%, and in some cases up to 50% for reactive dyes—remains unfixed during the dyeing

process and is released into wastewater (Drumond et al. 2011; Pereira and Alves 2012). Even very low concentrations of these dyes (< 1 ppm) can impart strong coloration, reduce light penetration, hinder photosynthesis, and cause oxygen depletion, thereby disrupting aquatic ecosystems (Javaid and Qazi 2019; Weldegebrieal 2020).

Conventional methods for dye removal—such as chemical oxidation, reduction, adsorption, coagulation, flocculation, and flotation—are often inefficient because they either lead to incomplete degradation, producing secondary toxic by-products, or generate large volumes of sludge that require additional disposal (Muhd Julkapli et al. 2014; Singh and Arora 2011; Saeed et al. 2018). In contrast, heterogeneous photocatalysis using semiconductor nanoparticles such as ZnO offers several advantages. It enables the complete mineralization of dyes into harmless products like CO_2, H_2O, and simple mineral acids (Kumar et al. 2014; Tripathi et al. 2025), can be driven by solar irradiation (making it energy-efficient and cost-effective), and avoids the generation of secondary waste, making it a sustainable solution for wastewater treatment.

Beyond photocatalysis, ZnO nanoparticles also display strong antibacterial and antifungal activity, making them useful for controlling pathogenic microorganisms that cause infectious diseases and food spoilage. This multifunctionality has prompted interest in developing green and sustainable synthesis methods for ZnO. While physical and chemical synthesis approaches are well established, they often require toxic reagents, harsh conditions, and high energy inputs. In contrast, biosynthesis using plant extracts has emerged as a promising alternative. This method offers several advantages: it is rapid, inexpensive, requires only simple laboratory facilities, uses eco-friendly precursors, and produces nanoparticles with high purity without introducing toxic by-products (Gawade et al. 2017). Such green-synthesized ZnO nanoparticles are therefore well suited for dual applications in environmental remediation—through photocatalytic degradation of dyes—and in biomedical or antibacterial applications.

In this study, zinc oxide (ZnO) nanoparticles were synthesized via two distinct green synthesis routes using saffron (Crocus sativus) floral extracts to examine the influence of synthesis method and extract type on photocatalytic performance. In the first approach, ZnO nanoparticles (Z2) were obtained from saffron petal extract via the sol–gel method, while in the second (Z4), anther extract was employed through the co-precipitation method. These environmentally benign processes avoid hazardous chemicals and support sustainable nanomaterial production. The structural, morphological, and chemical properties of both ZnO samples were characterized using X-ray diffraction (XRD), Raman spectroscopy, high-resolution transmission electron microscopy (HR-TEM), and X-ray photoelectron spectroscopy (XPS), confirming the presence of high-purity nanoscale crystallites with well-defined morphology. Photocatalytic activities were evaluated under direct natural sunlight using methylene blue (MB), rhodamine B (RhB), and crystal violet (CV) as model pollutants. The comparative study highlights how the extract source and synthesis pathway influence the degradation efficiency, demonstrating the potential of green-synthesized ZnO nanoparticles as effective photocatalysts for environmental remediation.

Materials and methods

Materials

Zinc nitrate hexahydrate ($Zn(NO_3)_2{\cdot}6H_2O$, 99.99% purity) and ammonium hydroxide (NH_4OH, 99% purity) were purchased from Sigma-Aldrich and used as received without additional purification. Fresh saffron (Crocus sativus L) flowers were collected from the Pampore region in Jammu and Kashmir, India. The anthers and petals were separated by hand, thoroughly washed with distilled water, and used for extract preparation.

Preparation of saffron flower extracts

Fresh saffron (Crocus sativus L.) flowers were obtained from the Pampore region of Jammu & Kashmir, India, during the harvesting season. The flowers were washed thoroughly with distilled water to remove dust and other surface impurities. The anthers and petals were manually separated and air-dried at room temperature in the shade for 24 h to reduce surface moisture.

To prepare the aqueous extracts, 5 g each of dried saffron flower anthers and petals were separately washed thoroughly and sonicated to remove any adhering dirt and soil particles. Each sample was then mixed with 150 mL of distilled water and heated at 70 °C for one hour with constant stirring to facilitate the extraction of bioactive compounds. After heating, the mixtures were allowed to cool naturally to room temperature. The solutions were then filtered through muslin cloth to remove solid residues, yielding clear aqueous extracts. These filtrates were used immediately in the green synthesis of ZnO nanoparticles, serving as natural reducing, capping, and chelating agents in the co-precipitation process.

Green synthesis of ZnO nanoparticles using saffron flower anther (Z2) and petal (Z4) extract: co-precipitation method

Zinc nitrate hexahydrate ($Zn(NO_3)_2{\cdot}6H_2O$, 99.99% purity) and ammonium hydroxide (NH_4OH, 99% purity) were both purchased from Sigma-Aldrich. First, zinc nitrate hexahydrate was weighed according to the required stoichiometric calculations and dissolved in 40 mL of double-distilled water. This solution was then

stirred continuously at room temperature for approximately 30 min. Subsequently, 100 mL of aqueous extract obtained from saffron flower anthers was added dropwise to the solution, acting as a natural chelating and stabilizing agent. The pH was then monitored, and ammonium hydroxide (NH_4OH) was added dropwise until a pH of 10 or higher was achieved. Ammonium hydroxide (NH_4OH) was employed as a mild precipitating and pH-controlling agent. The gradual release of OH^- ions facilitates the formation of Zn $(OH)_2$ intermediates according to:

$$Zn^{2+} + 2OH^- \rightarrow Zn\ (OH)_2$$

Furthermore, ammonia can coordinate with Zn^{2+} to form $[Zn\ (NH_3)\ _4]\ ^{2+}$ complexes, regulating nucleation and particle growth. Upon drying or thermal treatment, Zn $(OH)_2$ dehydrates to ZnO:

$$Zn\ (OH)_2 \rightarrow ZnO + H_2O.$$

The formation of ZnO nanoparticles proceeds via a hydroxide-mediated precipitation pathway. In aqueous solution, zinc nitrate dissociates to provide Zn^{2+} ions:

$$Zn\ (NO_3)_2 \rightarrow Zn^{2+} + 2NO_3{}^-$$

Upon addition of ammonium hydroxide (NH_4OH), hydroxide ions are generated according to:

$$NH_4OH \rightleftharpoons NH_4{}^+ + OH^-$$

The released OH^- ions react with Zn^{2+} to form zinc hydroxide intermediates:

$$Zn^{2+} + 2OH^- \rightarrow Zn\,(OH)_2$$

Under ammoniacal conditions, transient zinc–ammine complexes may form, which can regulate nucleation and particle growth. Upon drying or thermal treatment, Zn $(OH)_2$ undergoes dehydration to yield ZnO nanoparticles:

$$Zn\ (OH)_2 \rightarrow ZnO + H_2O$$

The reaction mixture was heated to 70 °C and maintained under stirring for 2 h. The precipitate formed was centrifuged at 9,000 rpm for 5 min and washed five times—twice with double-distilled water, once with ethanol, and again twice with double-distilled water. The product was then dried in an oven at 90 °C for 12 h, followed by calcination in a muffle furnace at 600 °C for 2 h. The obtained ZnO nanoparticles were finally ground using a mortar and pestle to obtain a fine homogeneous powder, as shown in Fig. 1.

A similar synthesis procedure was followed for the petal extract, with 100 mL of aqueous extract obtained from saffron flower petals replacing the anther extract in

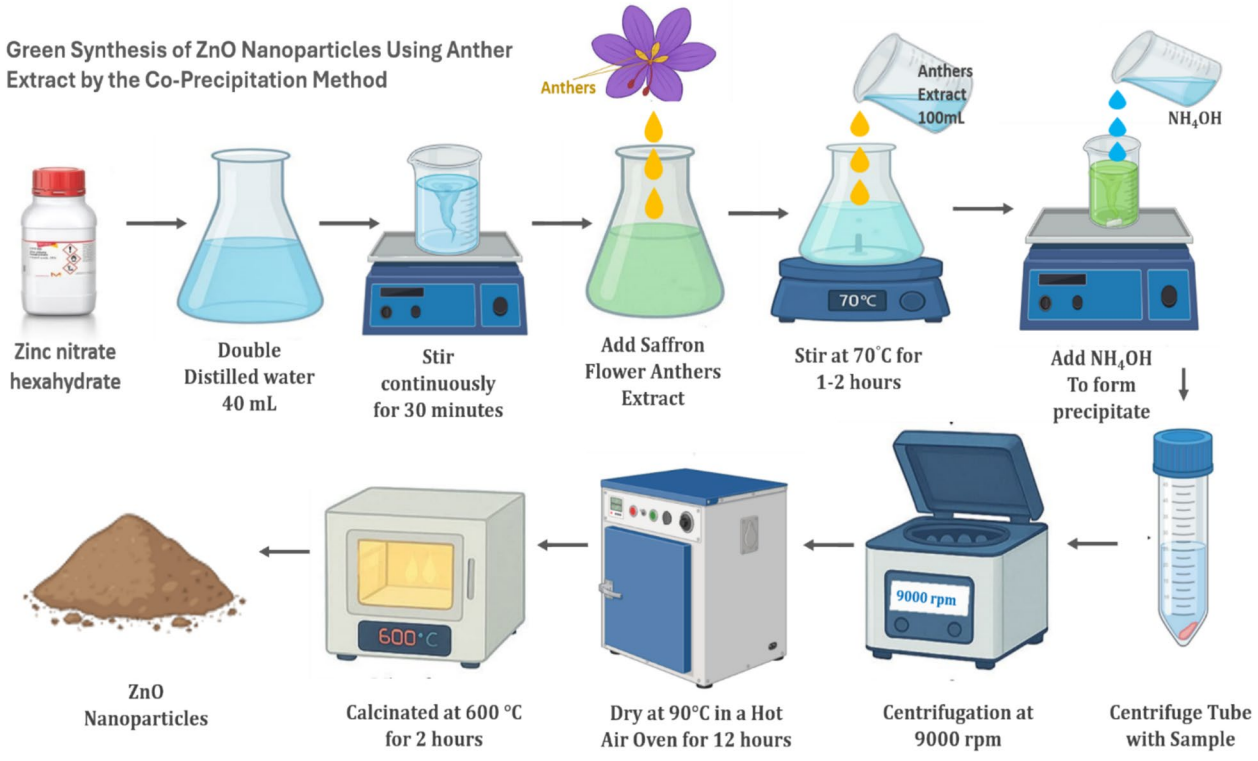

Fig. 1 Green Synthesis of ZnO Nanoparticles Using Anthers Extract by the Co-Precipitation Method

the initial step, as shown in Fig. 2. The rest of the reaction conditions, including pH adjustment, heating, centrifugation, washing, drying, and calcination, remained the same, ensuring that any observed variations in nanoparticle properties could be attributed primarily to the different phytochemical compositions of the petals and anthers.

Results and Discussion

XRD analysis

The XRD patterns of ZnO nanoparticles synthesized via the green co-precipitation route using (a) anther extract and (b) petal extract are essentially identical and match the hexagonal wurtzite phase of ZnO (space group $P6_3mc$), in agreement with the standard ICDD/JCPDS card no. 36–1451 (Jayswal and Moirangthem 2018) shown in Fig.3. The characteristic reflections appear at $2\theta \approx 31.7°$ (100), 34.4° (002), 36.2° (101; most intense), 47.5° (102), 56.6° (110), 62.8° (103), 66.4° (200), 67.9° (112), and 69.1°–72.6° (201/202/204, weak), consistent with previously reported wurtzite ZnO diffraction data (Özgür et al. 2005). No detectable impurity peaks from Zn $(OH)_2$ or other zinc phases were observed, confirming the formation of phase-pure ZnO in both cases (Kołodziejczak-Radzimska and Jesionowski 2014a). The nearly identical relative intensities suggest no strong preferred orientation, and the comparable peak widths indicate similar crystallite sizes and micro strain for anther- and petal-derived samples; any small broadening differences can be explained by phytochemical-mediated nucleation and growth effects rather than changes in crystal structure (Cullity 1978). Overall, the plant part used (anther vs. petals) does not alter the crystal phase or lattice symmetry but may subtly influence crystallite size distribution and defect density, consistent with earlier findings for plant-extract-mediated ZnO synthesis (Kołodziejczak-Radzimska and Jesionowski 2014a).

Raman analysis

The Raman spectra of the green-synthesized ZnO made with anther extract (Z2) and petal extract (Z4) both show the fingerprints of wurtzite ZnO in Fig. 4. In (Z2), the main peaks occur at 205, 275, 331, 436.9, 577, and 642 cm^{-1}; in Z4, they are at 201, 272, 325, 428, 570, and 642 cm^{-1}. The intense band near 437 cm^{-1} (Z2: 436.9; Z4: 428) is the E_2(high) mode of wurtzite ZnO; its downshift by ~ 9 cm^{-1} in Z4 is consistent with tensile micro strain and/or phonon-confinement effects typical for smaller/defective ZnO nanocrystals (canonical bulk E_2(high) ≈ 437 cm^{-1}) (Mora-Fonz et al. 2015). The features at ~ 331 cm^{-1} (Z2) and ~ 325 cm^{-1} (Z4) correspond to the E_2(high)–E_2(low) combination, while ~ 205 cm^{-1} (Z2) and ~ 201 cm^{-1} (Z4) are the $2E_2$(low) overtone; both are standard second-order ZnO bands. The peaks at ~ 275–272 cm^{-1}arise from TA(M) + LA(M) combinations, again expected for wurtzite ZnO (Guo et al. 2010). The bands in

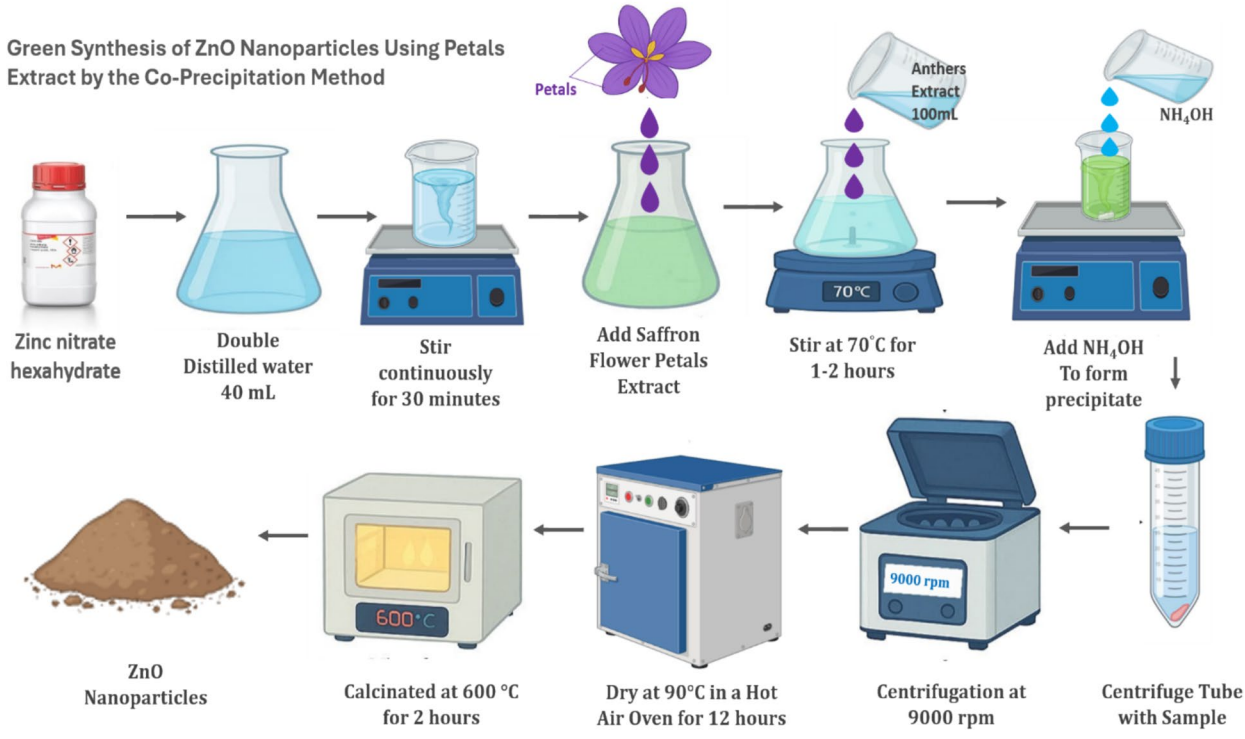

Fig. 2 Green Synthesis of ZnO Nanoparticles Using Petals Extract by the Co-Precipitation Method

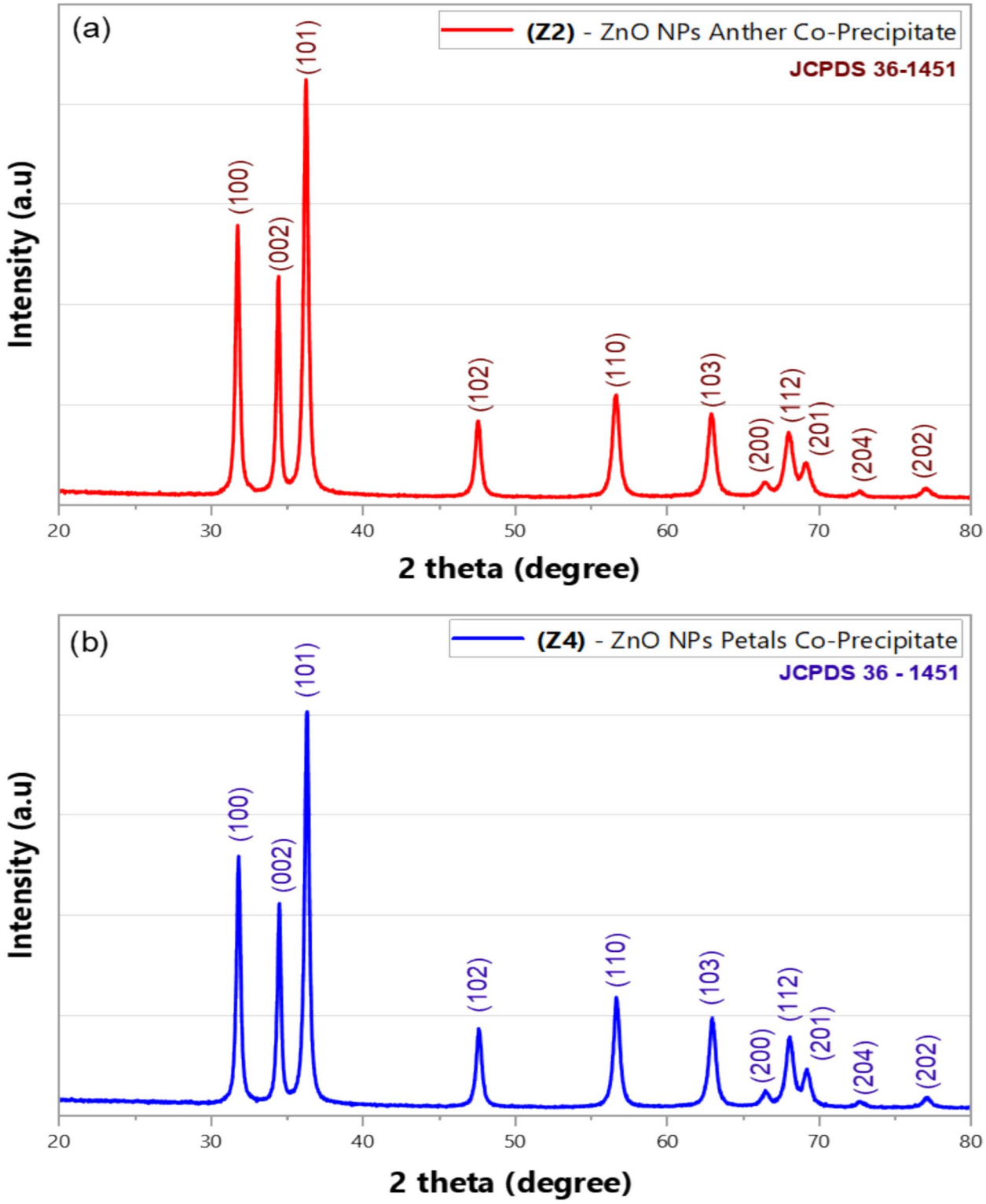

Fig. 3 XRD graphs of green-synthesized ZnO nanoparticles (**a**), anther extract (Z2) (**b**), and petal extract (Z4)

the LO region differ most: Z2 shows A_1(LO) at ~ 577 cm^{-1}, whereas Z4 is at ~ 570 $cm^{-1}$with lower relative intensity; LO-mode position/intensity are highly sensitive to point defects (oxygen vacancies V_O, zinc interstitials Zn_i) and resonance effects stronger, slightly higher-wavenumber LO features generally indicate greater defect concentration and different carrier–phonon coupling, so Z2 likely contains more V_O/Zn_i than Z4 (Bura et al. 2025).

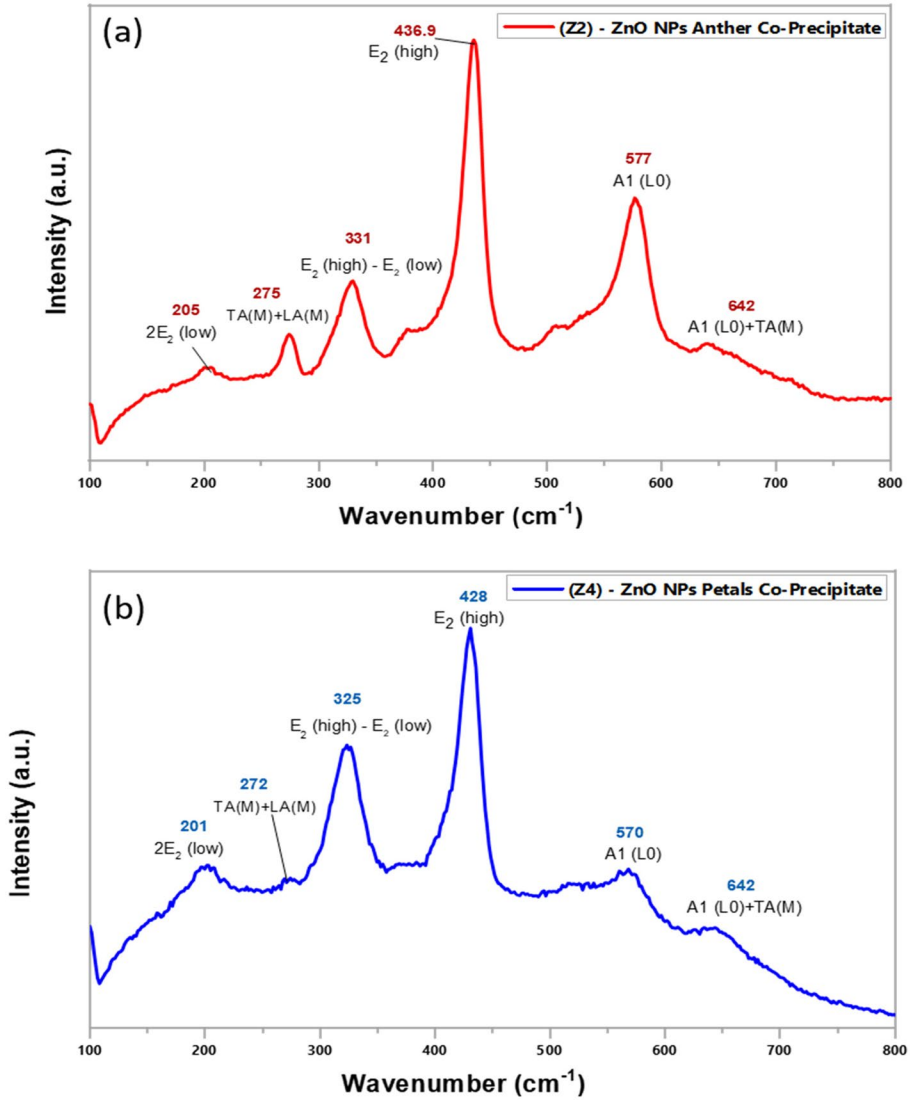

Fig. 4 Raman graphs of green-synthesized ZnO nanoparticles (**a**), anther extract (Z2) (**b**), and petal extract (Z4)

The weak shoulder near ~ 642 cm^{-1}in both samples is attributable to A_1(LO) + TA(M) multiphonon scattering (Guo et al. 2010). Overall, both extracts yield phase-pure wurtzite ZnO, but Z4 is more downshifted in E_2(high) and LO modes (428/570 cm^{-1}) pointing to higher tensile strain and/or smaller phonon-coherence length with fewer LO-active defects than (Z2); by contrast, (Z2)'s stronger ~ 577 cm^{-1}LO band suggests more native defects (V_O/Zn_i) introduced by its phytochemical environment during growth (Yoshikawa et al. 2008).

XPS analysis

The XPS analysis of ZnO nanoparticles synthesized by the two green routes (anther extract, Z2, and petal extract, Z4) reveals the characteristic Zn and O signals of wurtzite ZnO with no significant impurity peaks, confirming the purity of both samples in Figs. 5 and 6. In both spectra, the Zn 2p region displays two strong peaks at ~ 1021 eV (Zn $2p_{3/2}$) and ~ 1044 eV (Zn $2p_{1/2}$) with a spin–orbit splitting of ~ 23 eV, consistent with the Zn^{2+} oxidation state (Biesinger 2017; Moulder 1992).

The main differences are observed in the O 1 s region: Z2 shows a dominant lattice oxygen peak at ~ 530 eV accompanied by a pronounced shoulder at ~ 531–532 eV, which is attributed to oxygen vacancies, hydroxyl groups, and chemisorbed oxygen species (Luque-Morales et al. 2021; Wang et al. 2018). In contrast, Z4 also exhibits the lattice oxygen feature at ~ 530 eV but with a weaker high-binding-energy component, suggesting a lower concentration of surface defects. This variation can be traced back to differences in the phytochemical composition of the two extracts, which affect nucleation and defect passivation during ZnO formation (Basnet et al. 2018). The stronger defect-related O 1 s intensity in Z2 implies

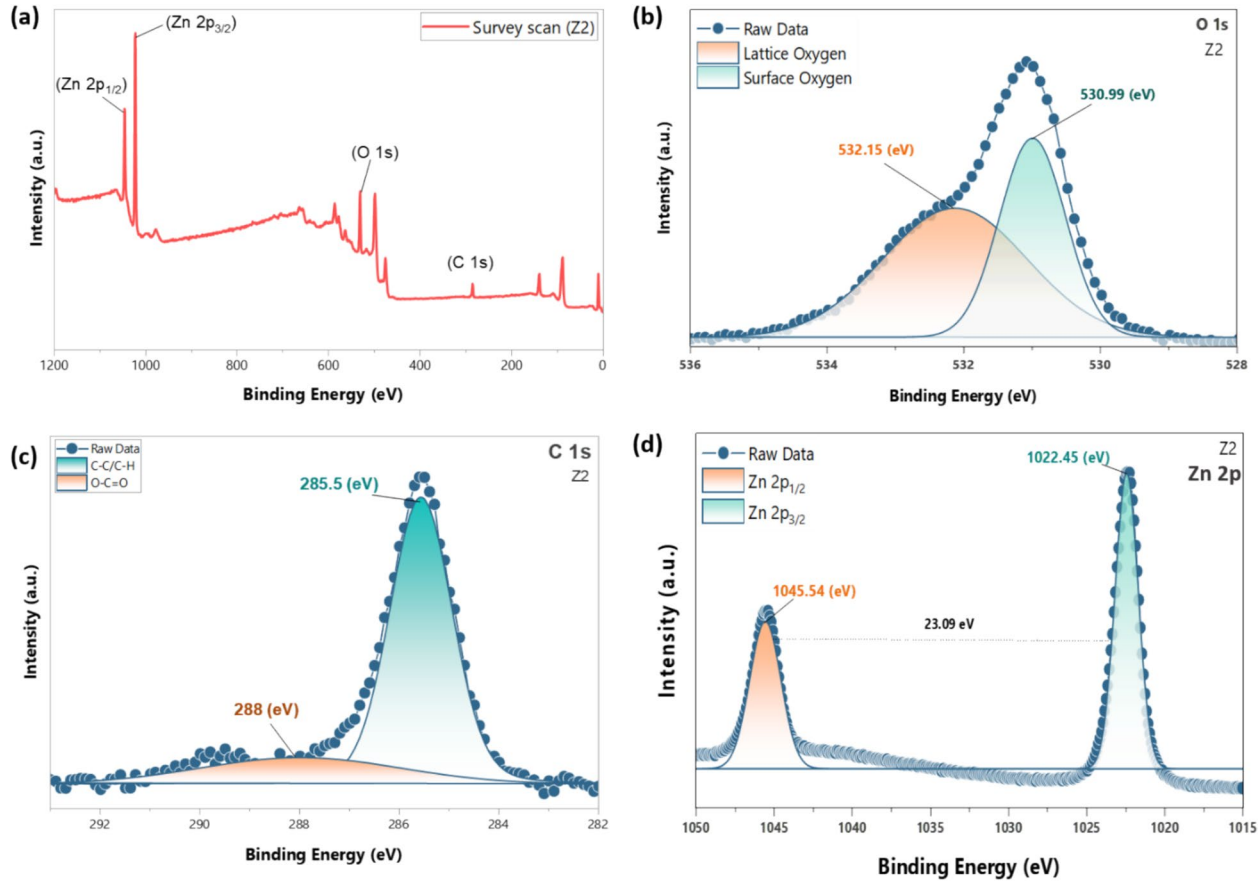

Fig. 5 XPS spectra of ZnO nanoparticles synthesized using saffron anther extract (Z2): (**a**) survey spectrum, (**b**) high-resolution O 1 s spectrum, (**c**) high-resolution C 1 s spectrum, and (**d**) high-resolution Zn 2p spectrum

a higher density of oxygen vacancies and Zn interstitials, known to enhance photocatalytic activity through improved charge trapping and reactive oxygen species generation, whereas Z4 may exhibit relatively lower photocatalytic reactivity but improved structural and chemical stability (Luque-Morales et al. 2021; Wang et al. 2018). Overall, the comparative XPS results highlight how the choice of biological precursor in green synthesis not only dictates particle formation but also tailors defect chemistry at the nanoscale, thereby tuning functional performance.

HR-TEM analysis

The HRTEM analysis of the ZnO nanoparticles synthesized via the green route reveals their nanocrystalline nature, with particles exhibiting well-resolved lattice fringes. The measured interplanar spacing of ~ 0.26 nm corresponds to the (002) plane of the hexagonal wurtzite ZnO structure (JCPDS card No. 36–1451), in agreement with earlier reports (Ong et al. 2018; Chemingui et al. 2019). The nanoparticles display quasi-spherical morphology in (Fig. 7a-b) with an average particle size of ~ 26 nm, in (Fig. 7c), suggesting that biomolecules present in the plant extract regulate the nucleation and growth process, thereby limiting excessive agglomeration (Green 2023). The SAED pattern further supports the high crystallinity of the ZnO nanoparticles, showing sharp and concentric diffraction rings that can be indexed to the (100), (002), (101), and (110) planes of wurtzite ZnO in (Fig.7d). The absence of diffuse halos in the diffraction pattern confirms the negligible presence of amorphous phases. Together, the HRTEM and SAED results provide direct evidence that the green synthesis method yields highly crystalline ZnO nanoparticles with well-defined lattice ordering, making them suitable for applications where crystallinity plays a key role, such as photocatalysis and optoelectronics (Kavitha et al. 2014).

Photocatalytic analysis of Z2

The photocatalytic activity of the green-synthesized ZnO nanoparticles (Z2) was evaluated using three organic dyes—methylene blue (MB), rhodamine B (RhB), and crystal violet (CV)—under visible light irradiation. The UV–Visible absorption spectra (Fig. 8a–c)) revealed a gradual decrease in the main absorption bands of all three dyes with increasing irradiation time, confirming

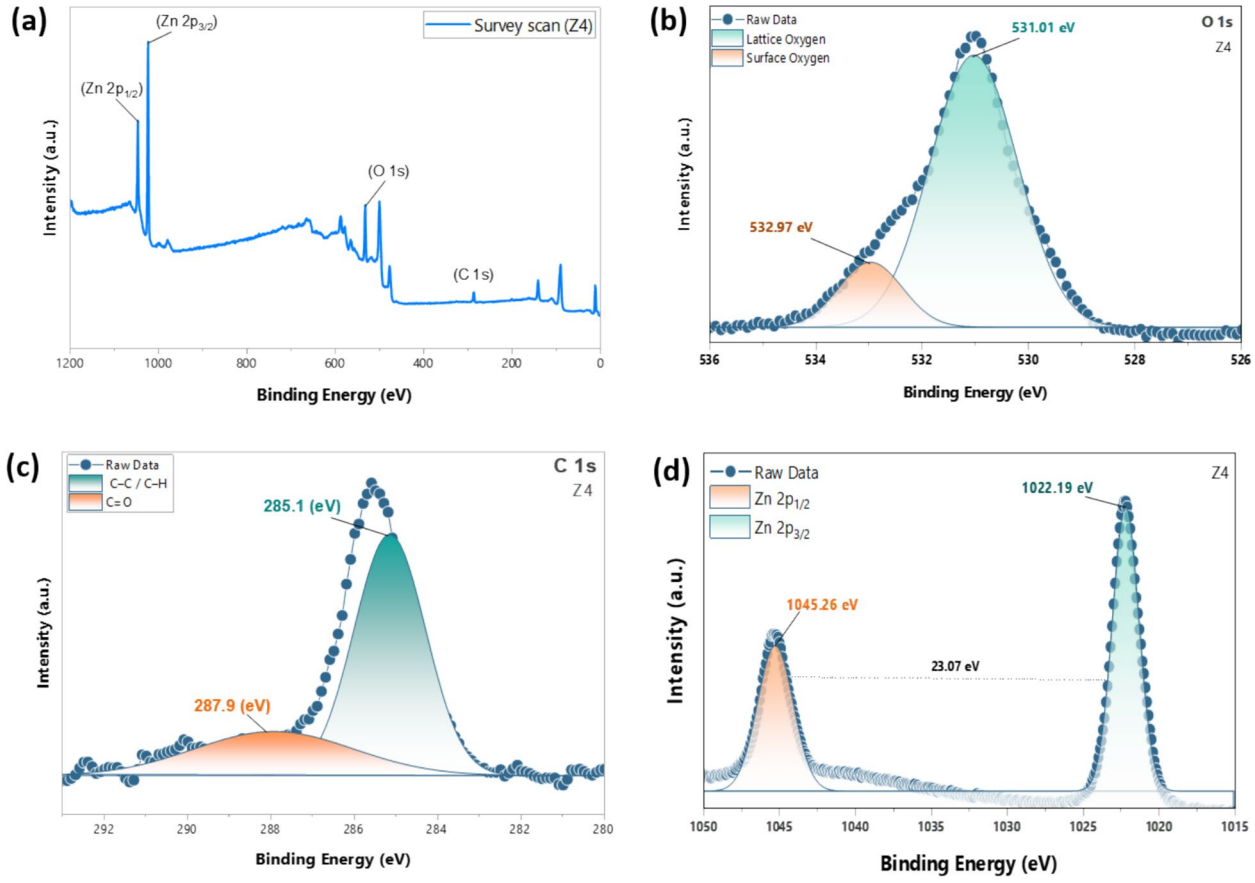

Fig. 6 XPS spectra of ZnO nanoparticles synthesized using saffron anther extract (Z4): (**a**) survey spectrum, (**b**) high-resolution O 1 s spectrum, (**c**) high-resolution C 1 s spectrum, and (**d**) high-resolution Zn 2p spectrum

the photocatalytic degradation of the pollutants. The normalized concentration plots (C/C_0 vs. time, (Fig. 8d–f)) indicated that ZnO effectively decomposes all dyes, with CV exhibiting the fastest decline, followed by MB, while RhB showed the slowest degradation (Fig. 8g–i)) Quantitative analysis using the pseudo-first-order Langmuir–Hinshelwood model (Fig. 8j–l)) yielded apparent rate constants of 0.00957 min^{-1} for MB, 0.00631 min^{-1} for RhB, and 0.0122 $min^{-1}$for CV, corresponding to half-lives of ~ 72.4 min, ~ 109.8 min, and ~ 56.8 min, respectively. The linearity of the $\ln(C_0/C)$ versus time plots validates the first-order kinetic model, confirming that the process is surface-reaction limited rather than diffusion-controlled. The higher rate constant of CV compared to MB and RhB suggests stronger adsorption and interaction at oxygen-vacancy sites and surface defect states of ZnO, which facilitate charge transfer and enhance reactive oxygen species (ROS) generation (Konstantinou and Albanis 2004; Chong et al. 2010; Cuscó et al. 2007). In the case of RhB, the slower degradation rate is consistent with previous studies and can be attributed to a more complex degradation pathway involving stepwise N-deethylation, which produces intermediate species and leads to a characteristic blue shift in the absorption spectrum during irradiation (Suneel et al. 2026). These findings highlight the importance of surface defect-mediated processes in ZnO photocatalysis, where oxygen vacancies play a crucial role in prolonging charge carrier lifetime and enhancing ROS formation (Ansari et al. 2024a; Rahman et al. 2013a). Overall, the green-synthesized ZnO nanoparticles demonstrate efficient photocatalytic performance against structurally diverse dyes, supporting their potential application in wastewater treatment, while the obtained rate constants are comparable to or higher than those reported for other plant-extract-assisted ZnO systems (Ansari et al. 2024a, 2024b; Rahman et al. 2013b).

Photocatalytic analysis of Z4

The photocatalytic performance of the green-synthesized ZnO nanoparticles (Z4) was investigated against three model dyes—methylene blue (MB), rhodamine B (RhB), and crystal violet (CV)—under visible light irradiation. The UV–Visible absorption spectra (Fig. 9a–c) showed a progressive decrease in the characteristic absorption peaks of the dyes with increasing irradiation time, confirming efficient photocatalytic degradation. The

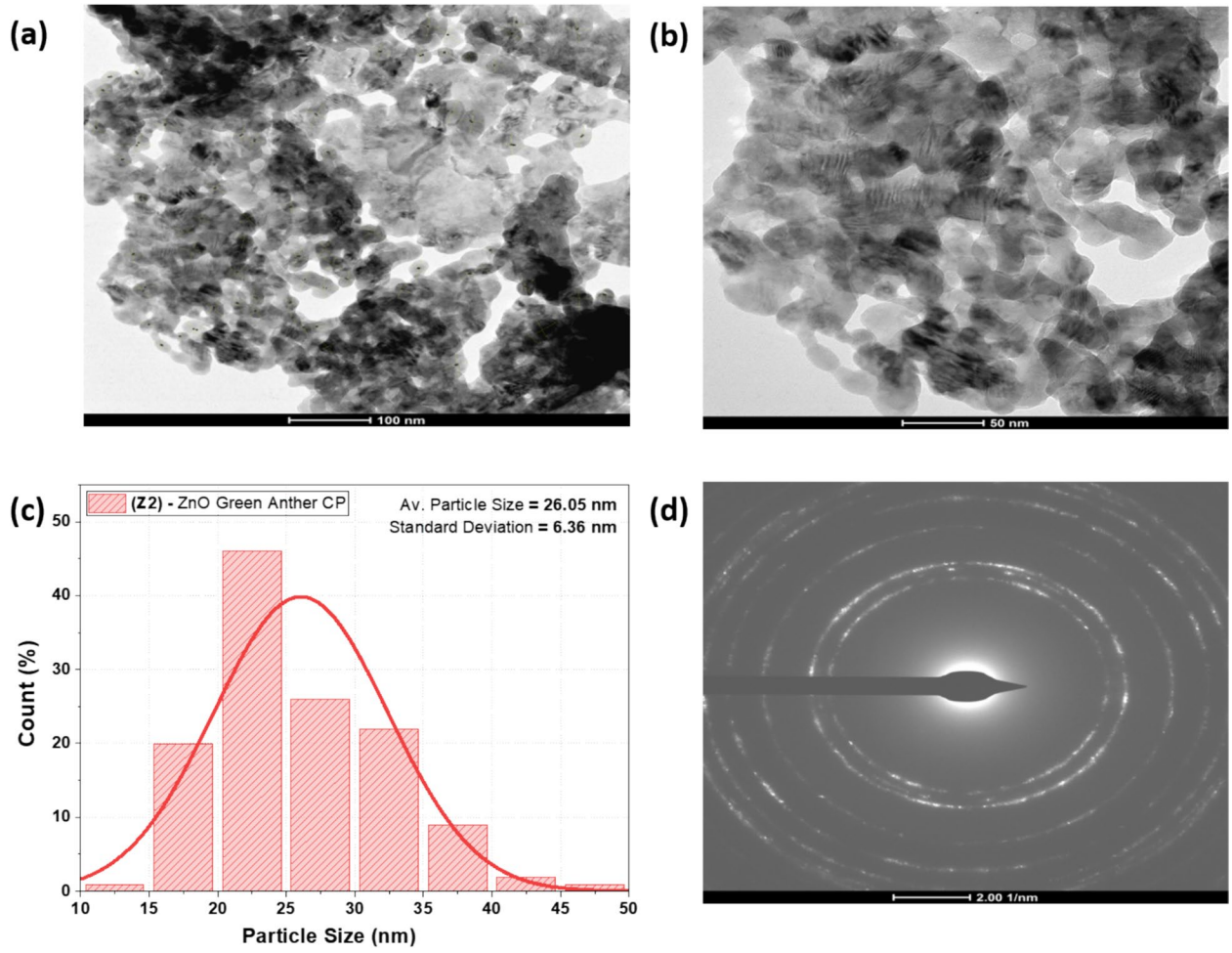

Fig. 7 HRTEM analysis of ZnO nanoparticles: (**a**–**b**) representative images showing spherical nanoparticles with sizes ranging from ~ 50 to 100 nm, (**c**) particle size distribution histogram indicating the average particle size, and (**d**) selected area electron diffraction (SAED) pattern confirming the polycrystalline nature of the material

concentration decay curves (C/C_0 vs. time, (Fig. 9d–f) and degradation efficiency plots (Fig. 9g–i) further demonstrated the activity of ZnO, with MB undergoing the fastest degradation, followed by CV and RhB. Kinetic fitting of the data with the pseudo-first-order Langmuir–Hinshelwood model (Fig. 9j–l) yielded apparent rate constants of 0.01526 min^{-1} for MB, 0.00674 min^{-1} for RhB, and 0.00771 $min^{-1}$for CV, corresponding to half-lives of ~ 45.4 min, ~ 102.8 min, and ~ 89.9 min, respectively. The linearity of the $\ln(C_0/C)$ versus time plots validates the first-order model, indicating that the degradation is surface-reaction limited rather than diffusion-controlled. The comparatively higher rate of MB degradation may be attributed to its stronger adsorption and charge transfer interactions at ZnO defect sites. In contrast, the slower degradation of RhB is consistent with its multi-step N-deethylation pathway, which produces intermediate species before full mineralization. These findings highlight the role of oxygen vacancies and defect-mediated charge separation in ZnO photocatalysis (Konstantinou and Albanis 2004; Chong et al. 2010; Cuscó et al. 2007; Yang et al. 2020; Zhang et al. 2007). Importantly, the obtained rate constants are comparable to or higher than those reported for other plant-extract-assisted ZnO nanoparticles, such as hibiscus-extract ZnO (k ≈ 0.004–0.008 $min^{-1}$for MB) (Hussein et al. 2025), and hydrothermal green-synthesized ZnO (k ≈ 0.005–0.010 $min^{-1}$for MB and RhB) (Trandafilović et al. 2017), underlining that the present bio-synthesized ZnO nanoparticles exhibit competitive or superior photocatalytic efficiency. Taken together, these results demonstrate that green ZnO systems not only provide a sustainable synthetic route but also deliver high photocatalytic activity, supporting their practical potential in wastewater treatment applications (Tables 1 and 2).

A comparison of the photocatalytic performance of ZnO nanoparticles synthesized with saffron anther extract (Z2) and saffron petal extract (Z4) highlights the strong influence of the plant precursor on degradation kinetics. For MB, Z4 exhibited a significantly higher rate

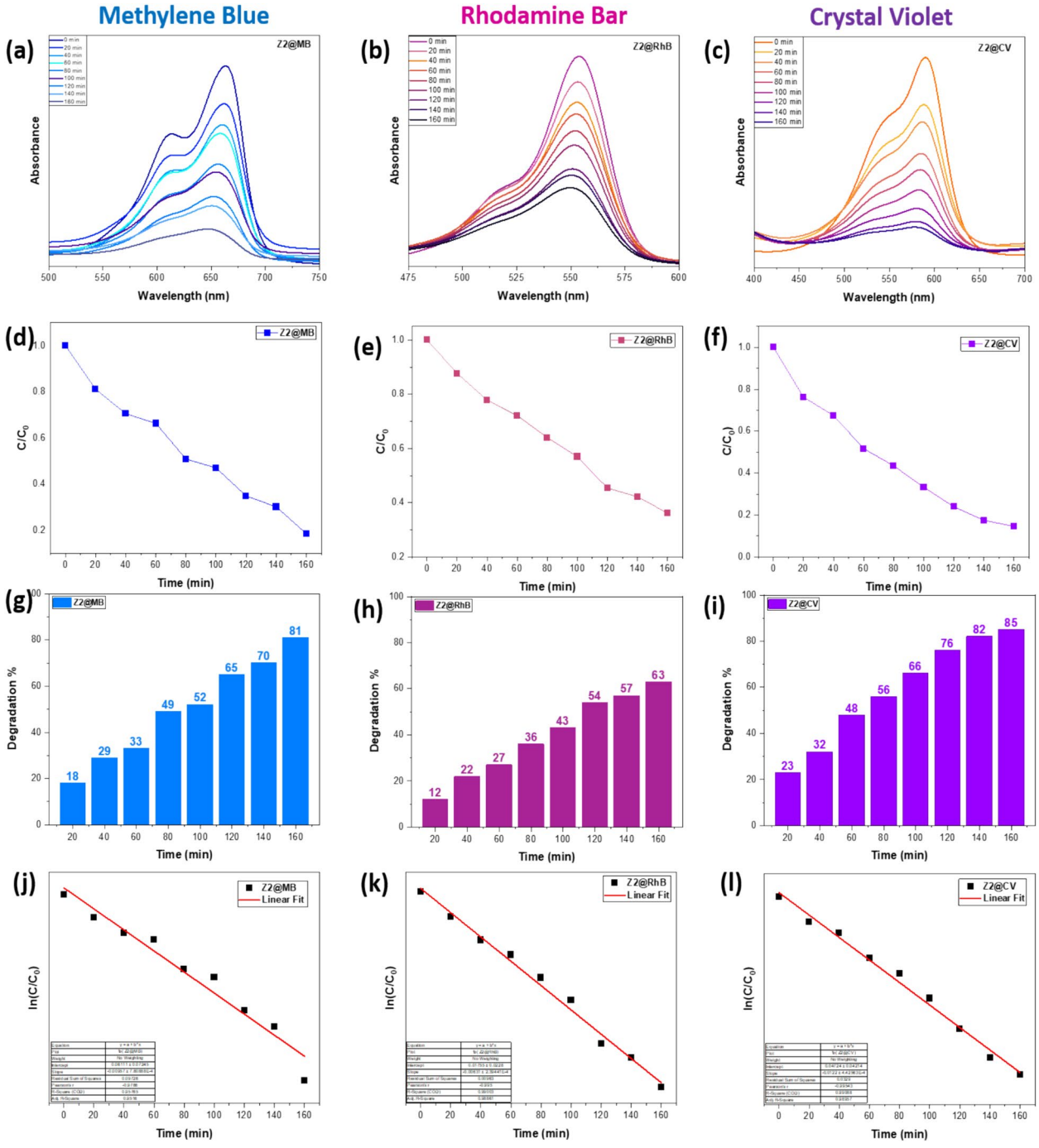

Fig. 8 Photocatalytic performance of ZnO nanoparticles synthesized using saffron anther extract (Z2): (**a**–**c**) UV–Vis absorbance spectra of MB, RhB, and CV as a function of irradiation time; (**d**–**f**) corresponding C/C_0 vs. time plots; (**g**–**i**) degradation efficiency of the three dyes with time; and (**j**–**l**) pseudo-first-order kinetic plots (ln C/C_0 vs. time)

constant (0.01526 min^{-1}, t½ ≈ 45.4 min) compared to Z2 (0.00957 min^{-1}, t½ ≈ 72.4 min), suggesting that the petal-derived ZnO possesses more favorable surface states for MB adsorption and charge transfer.

In contrast, Z2 outperformed Z4 in CV degradation, with k = 0.0122 min^{-1} (t½ ≈ 56.8 min) versus 0.00771 min^{-1} (t½ ≈ 89.9 min), indicating that the anther-derived ZnO provides more active defect sites for interaction with CV molecules. For RhB, both samples showed comparable activity (Z2: 0.00631 min^{-1}; Z4: 0.00674 min^{-1}), consistent with its multi-step N-deethylation mechanism that depends less on surface chemistry. These results demonstrate that even under identical co-precipitation conditions, the phytochemical composition

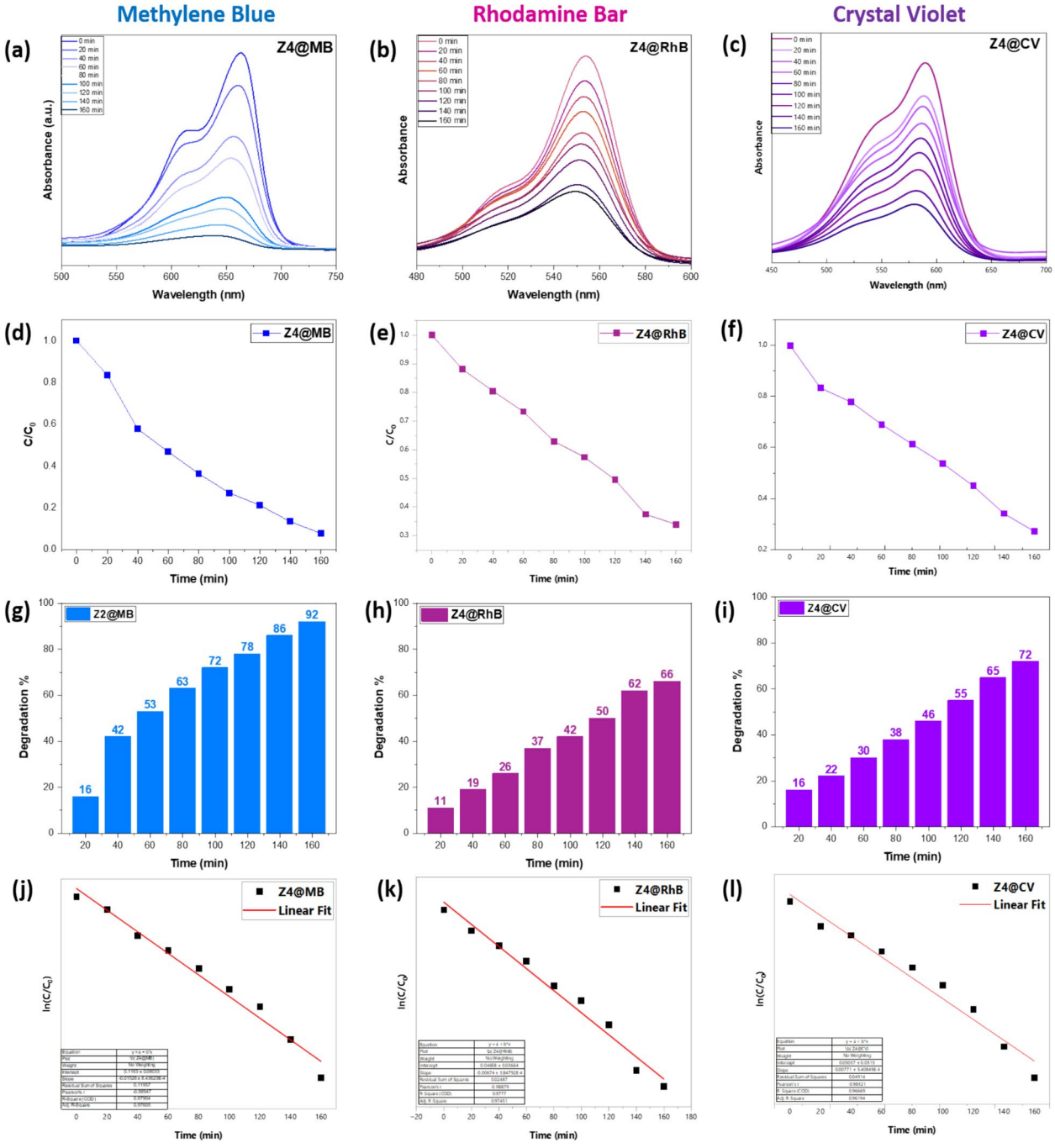

Fig. 9 Photocatalytic performance of ZnO nanoparticles synthesized using saffron petal extract (Z4): (**a**–**c**) UV–Vis absorbance spectra of MB, RhB, and CV as a function of irradiation time; (**d**–**f**) corresponding C/C_0 vs. time plots; (**g**–**i**) degradation efficiency of the three dyes with time; and (**j**–**l**) pseudo-first-order kinetic plots (ln C/C_0 vs. time)

of the chosen extract (anther vs. petal) can tailor ZnO nanoparticles' properties, leading to dye-specific variations in photocatalytic efficiency. The observed variation in crystallite size and photocatalytic efficiency between the anther- and petal-mediated ZnO samples can be attributed to differences in phytochemical composition. Anther extracts are typically rich in proteins and nitrogen-containing biomolecules, which can coordinate Zn^{2+} ions and regulate nucleation kinetics, whereas petal extracts contain higher concentrations of polyphenols and anthocyanins that influence surface capping and defect formation. These variations affect surface properties, oxygen vacancy concentration, and charge carrier dynamics, ultimately impacting photocatalytic

Table 1 Comparison of the photocatalytic degradation potential of green-synthesized, plant-based zinc oxide nanoparticles against methylene blue dye with previously reported works

Plant Source	Dye	Dye used	Catalyst dose	Degradation %	Time Min	Source	References
Moringa oleifera	MB	1 × 10–5 M	0.06 g	80	60	UV light	(Adam et al. 2021)
Corymbia citriodora	MB	(50 mL,20 mg/L)	20 mg	83.45	90	Visible light	(Zheng et al. 2015)
Beta vulgaris	MB	5 ppm	20 mg	80	150	UV light	(Pavan Kumar et al. 2015)
Trigonella foenumgraecum	MB	2.0 × 10 5 M	25 mg	88.3	90	UV light	(Alshehri and Malik 2019)
Amomum longiligulare	MB	50 µM	1 mg	66	60	UV light	(Liu et al. 2020)
Secamone emetica	MB	20 ppm	100 mg	69.76	210	Sunlight	(Sowmiya et al. 2025)
Eranthemum roseum	MB	20 ppm	50 mg	65	50	Sunlight	(Adhavan et al. 2024)
Lupinus albus	MB	5 ppm	50 mg	47.55	190	UV light	(Mirza et al. 2023)
Cocos nucifera	MB	50 mg/L	0.25 mg/mL	84.29	60	Sunlight	(Rahman et al. 2022)
Cosmos caudatus	MB	10 ppm	0.05 g	81.5	75	UV light	(Riwayati et al. 2024)
Phyllanthus acidus	MB	0.05 mM	1.5 g/L	72	90	Simulated solar light	(Kandasamy et al. 2025)
Crocus Sativus Anther	MB RhB CV	10 ppm	0.1 g/L	81 63 85	160	Sunlight	This work
Crocus Sativus Petal	MB RhB CV	10 ppm	0.1 g/L	92 66 72	160	Sunlight	This work

Table 2 Summary of Methylene Blue, Rhodamine Dye, and Crystal Violet dye degradation percentage, irradiation time, rate constant, and R^2 value

Sample	Dye	Degradation %	Irradiation Time	Rate Constant min^{-1}	R^2 Value
ZnO NPs with Anther (Z2)	Methylene Blue	81	160 min	0.00957	0.95785
	Rhodamine Bar	63	160 min	0.00631	0.99003
	Crystal Violet	85	160 min	0.0122	0.99088
ZnO NPs with Petal (Z4)	Methylene BlueRhodamine BarCrystal Violet	92 66 72	160 min 160 min 160 min	0.01526 0.00674 0.0071	0.97904 0.97770 0.96669

performance. Such tunability underscores the importance of extract selection in green synthesis strategies for optimizing ZnO-based photocatalysts in wastewater treatment.

Under sunlight irradiation, ZnO absorbs photons with energy equal to or greater than its bandgap energy, resulting in the excitation of electrons from the valence band (VB) to the conduction band (CB), generating electron–hole (e^-/h^+) pairs:

$$ZnO + hv \rightarrow e^-(CB) + h^+(VB)$$

The photogenerated electrons react with dissolved oxygen to form superoxide radicals ($\bullet O_2^-$):

$$e^- + O_2 \rightarrow \bullet O_2^-$$

Meanwhile, the holes oxidize water molecules or hydroxide ions to produce hydroxyl radicals (•OH):

$$h^+ + H_2O \rightarrow \bullet OH + H^+$$

These reactive oxygen species (•OH and $\bullet O_2^-$) are highly oxidative and attack the dye molecules, leading to their mineralization into CO_2, H_2O, and smaller intermediates (Rahman et al. 2013a, 2013b).

The enhanced photocatalytic performance observed for Z2 compared to Z4 may be attributed to differences in phytochemical composition of saffron anther and petal extracts. Phytochemicals such as flavonoids and phenolic compounds act as capping and stabilizing agents, influencing particle size, surface defects, and oxygen vacancy concentration. These surface modifications can improve charge separation efficiency and reduce electron–hole recombination, thereby enhancing reactive oxygen species generation.

Additionally, dye-dependent degradation behavior may arise from differences in molecular structure, adsorption affinity, and charge interactions with the ZnO surface.

Conclusion

Zinc oxide (ZnO) nanoparticles were successfully synthesized via a green approach using saffron anther (Z2) and petal (Z4) extracts as bio-templates. Structural (XRD), vibrational (Raman), surface chemical (XPS), and morphological (HRTEM with SAED) characterizations confirmed the formation of highly crystalline wurtzite ZnO with nanoscale dimensions and surface oxygen-related defects, which are critical to their photocatalytic behavior. The photocatalytic degradation of three model dyes—methylene blue (MB), rhodamine B (RhB), and crystal violet (CV)—under visible light irradiation revealed distinct differences between the two synthesis routes. For Z2 (anther extract),

the rate constants were 0.00957 min^{-1} (MB), 0.00631 min^{-1} (RhB), and 0.0122 min^{-1} (CV), while for Z4 (petal extract), they were 0.01526 min^{-1} (MB), 0.00674 min^{-1} (RhB), and 0.00771 min^{-1} (CV). These results indicate that Z4 exhibited superior performance for MB and RhB degradation, whereas Z2 was more effective for CV removal. Such differences may be attributed to variations in the phytochemical composition of the petal and anther extracts, which influence nanoparticle size, surface chemistry, and defect density, thereby affecting charge separation and reactive oxygen species generation.

Overall, the study demonstrates that both saffron petals and anthers provide sustainable, low-cost routes for the green synthesis of ZnO nanoparticles with promising photocatalytic activity. Their selective efficiency toward different dyes suggests potential for tailoring nanomaterials through controlled extract choice, opening new avenues for eco-friendly wastewater treatment strategies. Future research should investigate a broader set of pollutants, assess photocatalyst reusability, and explore the scalability of this synthesis method for real-world environmental remediation.

Acknowledgements
We thank Sharda University for providing the funding to support this research.

Authors' contributions
Adil Hamid: Conceptualization, methodology, synthesis of materials, characterization, photocatalytic experiments, data analysis, data interpretation and manuscript writing. Babita Tripathi: characterization support and manuscript review. Mohit Sahni: Supervision, conceptual guidance, resources, funding acquisition, and critical revision of the manuscript.

Funding
Open access funding provided by Sharda University.

Data availability
No datasets were generated or analysed during the current study.

Declarations

Competing interests
The authors declare no competing interests.

Author details
[1]Department of Physics and Environmental Sciences, Sharda School of Engineering and Science, Sharda University, Greater Noida, Uttar Pradesh, India

Received: 8 December 2025 / Accepted: 9 March 2026
Published online: 24 March 2026

References

Adam F, Himawan A, Aswad M, Ilyas S, Heryanto, Anugrah MA, Tahir D (2021) Green Synthesis of Zinc Oxide Nanoparticles Using Moringa Oleifera l. Water Extract and Its Photocatalytic Evaluation. J Phys Conf Ser 1763(1):012002. https://doi.org/10.1088/1742-6596/1763/1/012002

Adhavan R, Selvam K, Prakash P, Manimegalai P, Kirubakaran D, Shivakumar MS (2024) Bioefficacy of Zinc oxide nanoparticle synthesis and their biological, environmental applications from *Eranthemum roseum*. Toxicol Rep 13:101758. https://doi.org/10.1016/j.toxrep.2024.101758

Alshehri AA, Malik MA (2019) Biogenic fabrication of ZnO nanoparticles using *Trigonella foenum-graecum* (fenugreek) for proficient photocatalytic degradation of methylene blue under UV irradiation. J Mater Sci Mater Electron 30(17):16156–16173. https://doi.org/10.1007/s10854-019-01985-8

Ansari N, Ali A, Akhtar MS, Hasan S, Khatoon T, Khan AR, Wabaidur SM, Rahman QI (2024a) Green synthesis of zinc oxide marigold shaped clusters using *Eucalyptus globulus* leaf extract as robust photocatalyst for dyes degradation under sunlight. Mater Sci Semicond Process 173:108087. https://doi.org/10.1016/j.mssp.2023.108087

Ansari N, Kavish Md, Wagay JA, Khan Z, Khan AR, Ahmed S, Rahman QI (2024b) Sustainable synthesis of ZnO nanostructures using *Ficus religiosa* leaf extract with enhanced photocatalytic and antibacterial activity. Mater Sci Eng B Solid-State Mater 310:117752. https://doi.org/10.1016/j.mseb.2024.117752

Baruah S, Jaisai M, Imani R, Nazhad MM, Dutta J (2010) Photocatalytic paper using zinc oxide nanorods. Sci Technol Adv Mater 11(5):055002. https://doi.org/10.1088/1468-6996/11/5/055002

Basnet P, Chanu TI, Samanta D, Chatterjee S (2018) A review on bio-synthesized zinc oxide nanoparticles using plant extracts as reductants and stabilizing agents. J Photochem Photobiol B Biol 183:201–221. https://doi.org/10.1016/j.jphotobiol.2018.04.036

Benny BP, Sarkar P, Varshney S, Hamzah FM (2025) Light and Dark Mediated Synthesis of Silver Nanoparticles from *Moringa Oleifera* Leaves and *Myristica Fragans* Seeds. *Macromolecular Symposia* :e70217. https://doi.org/10.1002/masy.70217

Biesinger MC (2017) Advanced analysis of copper X-ray photoelectron spectra. Surf Interface Anal 49(13):1325–1334. https://doi.org/10.1002/sia.6239

Buapoon S, Phuruangrat A, Thongtem T, Thongtem S (2021) AgBr Nanoparticles–ZnO Flowers Nanocomposites Used for Photodegradation of Methylene Blue Solution Illuminated by Ultraviolet-Visible Radiation. Inorg Nano-Met Chem 51(4):523–530. https://doi.org/10.1080/24701556.2020.1799397

Bura M, Gupta D, Kumar A, Aggarwal S (2025) Ar^+ implantation-induced tailoring of RF-sputtered ZnO films: structural, morphological, and optical properties. Beilstein J Nanotechnol 16:872–886. https://doi.org/10.3762/bjnano.16.66

Cullity BD (1978) "Elements of X-Ray Diffraction," Second ed, (Reading (Mass.) Menlo Park (Calif.) London [etc.]), Addison-Wesley publ

Chaudhuri SK, Malodia L (2017) Biosynthesis of Zinc Oxide Nanoparticles Using Leaf Extract of Calotropis Gigantea: Characterization and Its Evaluation on Tree Seedling Growth in Nursery Stage. Appl Nanosci 7(8):501–512. https://doi.org/10.1007/s13204-017-0586-7

Chemingui H, Missaoui T, Mzali JC, Yildiz T, Konyar M, Smiri M, Saidi N, Hafiane A, Yatmaz HC (2019) Facile green synthesis of zinc oxide nanoparticles (ZnO NPs): antibacterial and photocatalytic activities. Mater Res Express 6(10):1050b4. https://doi.org/10.1088/2053-1591/ab3cd6

Chong MN, Jin B, Chow CWK, Saint C (2010) Recent developments in photocatalytic water treatment technology: a review. Water Res 44(10):2997–3027. https://doi.org/10.1016/j.watres.2010.02.039

Cuscó R, Alarcón-Lladó E, Ibáñez J, Artús L, Jiménez J, Wang B, Callahan MJ (2007) Temperature dependence of raman scattering in ZnO. Phys Rev B 75(16):165202. https://doi.org/10.1103/PhysRevB.75.165202

Drumond Chequer FM, Junqueira D, De Oliveir DP (2011) Azo Dyes and Their Metabolites: Does the Discharge of the Azo Dye into Water Bodies Represent Human and Ecological Risks? Advances in Treating Textile Effluent P. Hauser, Ed., InTech. https://doi.org/10.5772/19872

Gawade VV, Gavade NL, Shinde HM, Babar SB, Kadam AN, Garadkar KM (2017) Green synthesis of ZnO nanoparticles by using *Calotropis procera* leaves for the photodegradation of methyl orange. J Mater Sci Mater Electron 28(18):14033–14039. https://doi.org/10.1007/s10854-017-7254-2

Green Synthesis of ZnO Nanoparticles Using Moringa Oleifera Leaf Extract for Efficient Photocatalytic Degradation of Organic Dyes (2023) Global NEST Journal. https://doi.org/10.30955/gnj.005411

Guo S, Du Z, Dai S (2010) Analysis of raman modes in Mn-doped ZnO nanocrystals. arXiv. https://doi.org/10.48550/ARXIV.1009.2870

Hussein H, Ibrahim SS, Khairy SA (2025) Green synthesis of ZnO nanoparticles using *Hibiscus sabdariffa* L: rapid Pb2+ ion removal, photocatalytic degradation of methylene blue, and biomedical applications. J Water Process Eng 69:106649. https://doi.org/10.1016/j.jwpe.2024.106649

Javaid R, Qazi UY (2019) Catalytic oxidation process for the degradation of synthetic dyes: an overview. IJERPH 16(11):2066. https://doi.org/10.3390/ijerph16112066

Jayswal S, Moirangthem RS (2018) "Thermal Decomposition Route to Synthesize ZnO Nanoparticles for Photocatalytic Application (Noida, India) p:020023. https://doi.org/10.1063/1.5052092

Kandasamy M, Suresh S, Rameshkumar P, Jayasree R, Sathishkumar P, Gunnasegaran P, Topare NS, Thambidurai S, Arumugam J, Jothilakshmi R, Pugazhenthiran N (2025) Green synthesis of ultrafine Zinc oxide nanoparticles for photocatalytic degradation of methylene blue dye: optimization and kinetic studies. Results Eng 27:105846. https://doi.org/10.1016/j.rineng.2025.105846

Kavitha MK, Jinesh KB, Philip R, Gopinath P, John H (2014) Defect engineering in ZnO nanocones for visible photoconductivity and nonlinear absorption. Phys Chem Chem Phys 16(45):25093–25100. https://doi.org/10.1039/C4CP03847A

Kołodziejczak-Radzimska A, Jesionowski T (2014a) Zinc Oxide—From Synthesis to Application: A Review. Materials 7(4):2833–2881. https://doi.org/10.3390/ma7042833

Konstantinou IK, Albanis TA (2004) TiO2-assisted photocatalytic degradation of Azo dyes in aqueous solution: kinetic and mechanistic investigations. Appl Catal B Environ 49(1):1–14. https://doi.org/10.1016/j.apcatb.2003.11.010

Kumar S, Ahlawat W, Bhanjana G, Heydarifard S, Nazhad MM, Dilbaghi N (2014) Nanotechnology-based water treatment strategies. j Nanosci Nanotech 14(2):1838–1858. https://doi.org/10.1166/jnn.2014.9050

Liu YC, Li J, Ahn J, Pu J, Rupa EJ, Huo Y, Yang DC (2020) Biosynthesis of Zinc oxide nanoparticles by one-pot green synthesis using fruit extract of *Amomum longiligulare* and its activity as a photocatalyst. Optik 218:165245. https://doi.org/10.1016/j.ijleo.2020.165245

Luque-Morales PA, Lopez-Peraza A, Nava-Olivas OJ, Amaya-Parra G, Baez-Lopez YA, Orozco-Carmona VM, Garrafa-Galvez HE, Chinchillas-Chinchillas MDJ (2021) ZnO semiconductor nanoparticles and their application in photocatalytic degradation of various organic dyes. Materials 14(24):7537. https://doi.org/10.3390/ma14247537

Mirza S, Hussaini AA, Öztürk G, Turgut M, Öztürk T, Tugay O, Ulukuş D, Yıldırım M (2023) Photocatalytic and antibacterial activities of ZnO nanoparticles synthesized from *Lupinus albus* and *Lupinus pilosus* plant extracts via green synthesis approach. Inorg Chem Commun 155:111124. https://doi.org/10.1016/j.inoche.2023.111124

Mohammadi Azar D, Feizbakhsh A, Panahi HA, Niazi A (2022) Fabrication of the novel CoS_2 /ZnO nanocomposites with photocatalysis properties and response surface methodology study. Int J Environ Anal Chem 102(19):8490–8502. https://doi.org/10.1080/03067319.2020.1853114

Mora-Fonz D, Buckeridge J, Logsdail AJ, Scanlon DO, Sokol AA, Woodley S, Catlow CRA (2015) Morphological features and band bending at nonpolar surfaces of ZnO. J Phys Chem C 119(21):11598–11611. https://doi.org/10.1021/acs.jpcc.5b01331

Moulder JF, Chastain J (eds) (1992) "Handbook of X-Ray Photoelectron Spectroscopy: A Reference Book of Standard Spectra for Identification and Interpretation of XPS Data", Update, (Eden Prairie. Perkin-Elmer Corporation, Minn)

Muhd Julkapli N, Bagheri S, Bee Abd Hamid S (2014) Recent advances in heterogeneous photocatalytic decolorization of synthetic dyes. Sci World J 2014:1–25. https://doi.org/10.1155/2014/692307

Ogunyemi SO, Abdallah Y, Zhang M, Fouad H, Hong X, Ibrahim E, Masum MMI, Hossain A, Mo J, Li B (2019) Green Synthesis of Zinc Oxide Nanoparticles Using Different Plant Extracts and Their Antibacterial Activity against *Xanthomonas Oryzae* Pv. Oryzae. Artif Cells Nanomed Biotechnol 47(1):341–352. https://doi.org/10.1080/21691401.2018.1557671

Ong CB, Ng LY, Mohammad AW (2018) A review of ZnO nanoparticles as solar photocatalysts: synthesis, mechanisms and applications. Renew Sustain Energy Rev 81:536–551. https://doi.org/10.1016/j.rser.2017.08.020

Özgür Ü, Alivov YI, Liu C, Teke A, Reshchikov MA, Doğan S, Avrutin V, Cho S-J, Morkoç H (2005) A comprehensive review of ZnO materials and devices. J Appl Phys 98(4):041301. https://doi.org/10.1063/1.1992666

Pavan Kumar MA, Suresh D, Nagabhushana H, Sharma SC (2015) *Beta vulgaris* aided green synthesis of ZnO nanoparticles and their luminescence, photocatalytic and antioxidant properties. Eur Phys J plus 130(6):109. https://doi.org/10.1140/epjp/i2015-15109-2

Pereira L, Alves M (2012) Dyes—Environmental Impact and Remediation. Environmental Protection Strategies for Sustainable Development, A. Malik and E. Grohmann, Eds., (Dordrecht), Springer Netherlands. p 111–162. https://doi.org/10.1007/978-94-007-1591-2_4

Poole-Wilson PA, Langer GA (1975) Effect of pH on Ionic Exchange and Function in Rat and Rabbit Myocardium. Am J Physiol 229(3):570–581. https://doi.org/10.1152/ajplegacy.1975.229.3.570

Rahman F, Majed Patwary MA, Bakar Siddique MA, Bashar MS, Haque MA, Akter B, Rashid R, Haque MA, Uddin AKMR (2022) Green synthesis of zinc oxide nanoparticles using *Cocos nucifera* leaf extract: characterization, antimicrobial, antioxidant and photocatalytic activity. R Soc Open Sci 9(11):220858. https://doi.org/10.1098/rsos.220858

Rahman QI, Ahmad M, Misra SK, Lohani M (2013a) Effective photocatalytic degradation of Rhodamine B dye by ZnO nanoparticles. Mater Lett 91:170–174. https://doi.org/10.1016/j.matlet.2012.09.044

Rahman QI, Ahmad M, Misra SK, Lohani MB (2013b) Hexagonal ZnO nanorods assembled flowers for photocatalytic dye degradation: growth, structural and optical properties. Superlattices Microstruct 64:495–506. https://doi.org/10.1016/j.spmi.2013.10.011

Rashad M, Shaalan NM, Abd-Elnaiem AM (2016) Degradation Enhancement of Methylene Blue on ZnO Nanocombs Synthesized by Thermal Evaporation Technique. Desalin Water Treat 57(54):26267–26273. https://doi.org/10.1080/19443994.2016.1163511

Riwayati I, Winardi S, Madhania S, Shimada M, Kusdianto (2024) Green Synthesis of ZnO Nanoparticles Using Cosmos Caudatus: Effects of Calcination Temperature and Precursor Type on Photocatalytic and Antimicrobial Activities. Results in Engineering 24:103594. https://doi.org/10.1016/j.rineng.2024.103594

Saeed M, Usman M, Haq AU (2018) Catalytic Degradation of Organic Dyes in Aqueous Medium, Photochemistry and Photophysics - Fundamentals to Applications, S. Saha and S. Mondal, Eds., InTech. https://doi.org/10.5772/intechopen.75008

Singh K, Arora S (2011) Removal of synthetic textile dyes from wastewaters: a critical review on present treatment technologies. Crit Rev Environ Sci Technol 41(9):807–878. https://doi.org/10.1080/10643380903218376

Singh NB, Monjur A, Kumar B, Varshney S, Susan MABH (2025) Revolutionizing Healthcare with Nanosensor Technology. RSC Adv 15(46):38774–38810. https://doi.org/10.1039/D5RA04412J

Sowmiya M, Selvam K, Shivakumar MS (2025) Sustainable fabrication of Zinc oxide nanoparticles using *Secamone emetica* leaf extract: biological and environmental applications. Journal of Natural Pesticide Research 12:100122. https://doi.org/10.1016/j.napere.2025.100122

Suneel S, Hasan MA, Khan D, Bano A, Iqbal A, Imran A, Rahman QI (2026) Evaluation of physiochemical properties of G-C3N4/ZnO composites with enhanced photocatalytic activity under sunlight irradiation. Mater Sci Eng B Solid-State Mater 324:119008. https://doi.org/10.1016/j.mseb.2025.119008

Trandafilović LV, Jovanović DJ, Zhang X, Ptasińska S, Dramićanin MD (2017) Enhanced photocatalytic degradation of Methylene Blue and Methyl Orange by ZnO:Eu nanoparticles. Appl Catal B Environ 203:740–752. https://doi.org/10.1016/j.apcatb.2016.10.063

Tripathi B, Surajbhan S. Varshney, Yahya MZA, Noor IM (2025) Development of a Bismuth-Based Metal–Organic Framework for Hydrogen Production. Macromolecular Symposia :e70180. https://doi.org/10.1002/masy.70180

Umar A, Hahn Y-B (2010) Metal Oxide Nanostructures and Their Applications. CA), American scientific publishers, Los Angeles

Varshney S, Chi L, Singh CV, Nogami J (2022) Atomic Structure of PbBr 2 Thin Films on Ag (111). Solid State Commun 343:114651. https://doi.org/10.1016/j.ssc.2022.114651

Wang J, Chen R, Xiang L, Komarneni S (2018) Synthesis, properties and applications of ZnO nanomaterials with oxygen vacancies: a review. Ceram Int 44(7):7357–7377. https://doi.org/10.1016/j.ceramint.2018.02.013

Weldegebrieal GK, Dube HH, Sibhatu AK (2023) Photocatalytic Activity of CdO/ZnO Nanocomposite for Methylene Blue Dye and Parameters Optimisation Using Response Surface Methodology. Int J Environ Anal Chem 103(18):6146–6168. https://doi.org/10.1080/03067319.2021.1949589

Weldegebrieal GK (2020) Synthesis method, antibacterial and photocatalytic activity of ZnO nanoparticles for azo dyes in wastewater treatment: a review. Inorg Chem Commun 120:108140. https://doi.org/10.1016/j.inoche.2020.108140

Yang J, Zhu H, Peng Y, Li P, Chen S, Yang B, Zhang J (2020) Photocatalytic performance and degradation pathway of Rhodamine B with TS-1/C3N4 composite under visible light. Nanomaterials 10(4):756. https://doi.org/10.3390/nano10040756

Yoshikawa M, Inoue K, Nakagawa T, Ishida H, Hasuike N, Harima H (2008) Characterization of ZnO nanoparticles by resonant raman scattering and cathodoluminescence spectroscopies. Appl Phys Lett 92(11):113115. https://doi.org/10.1063/1.2901159

Zhang L, Jiang Y, Ding Y, Povey M, York D (2007) Investigation into the antibacterial behaviour of suspensions of ZnO nanoparticles (ZnO nanofluids). J Nanopart Res 9(3):479–489. https://doi.org/10.1007/s11051-006-9150-1

Zheng Y, Fu L, Han F, Wang A, Cai W, Yu J, Yang J, Peng F (2015) Green biosynthesis and characterization of zinc oxide nanoparticles using *Corymbia citriodora* leaf extract and their photocatalytic activity. Green Chem Lett Rev 8(2):59–63. https://doi.org/10.1080/17518253.2015.1075069

Publisher's Note

Springer Nature remains neutral with regard to jurisdictional claims in published maps and institutional affiliations.